Inertial Properties of a Living Population for the Development of Biofidelic Headforms

Thomas A. Connor [a, b, c], Niall Colgan [d], Matt Stewart [c], Aisling Ní Annaidh [a] and Michael D. Gilchrist [*, a]

a) *School of Mechanical & Materials Engineering, University College Dublin, Belfield, Dublin 4, Ireland.*

b) *HP1 Technologies Ltd., Aycliffe Business Park, Durham Way S, Newton Aycliffe, UK.*

c) *Charles Owen and Co. Ltd., Royal Works, Croesfoel, Wrexham, UK.*

d) *School of Physics, NUI Galway, Ireland.*

*Corresponding Author: Email: michael.gilchrist@ucd.ie

Abstract

The aim of this study is to create a new database of human head physical properties based on a living adult population that can be used to inform the development of future biofidelic headforms. Relationships between head circumference and mass, as well as head moments of inertia and mass, are sufficiently linear to provide simple, yet accurate, values for the mass and inertia properties of differently sized heads. Physical data regarding the dimensions, mass, moments of inertia and centre of gravity location for the heads of 56 living adults were obtained using a non-invasive method based on computed tomography (CT) based finite element (FE) models. The CT data showed good agreement with published cadaver data and significantly less variation. The data set presented in this paper provides an important basis for more biofidelic future headform designs. The linear equations associated with this new primary dataset relate head circumference to head mass and moments of inertia: Head Mass = 0.18 * Head Circumference – 6.08 where mass is in kg and circumference is in cm, while I_{xx} = 79.88 * Head Mass – 132.88, I_{yy} = 81.70 * Head Mass – 128.38 and I_{zz} = 53.88 * Head Mass – 86.66 where I is moments of inertia in kg.cm^2 and mass in kg. The X, Y and Z axes correspond to forward, lateral and vertical directions and the X-Z plane corresponds to the mid-sagittal plane. These results represent the first published human head physical property data that is based on a living population, rather than cadaver data. These data are freely available to all and should serve to improve the biofidelity of standard headforms in terms of their mass and moments of inertia.

Keywords: Moment of inertia, oblique impact, rotational motion, angular acceleration

1. Introduction

Sports and automotive helmets are certified by carrying out simplified impacts in which a helmeted headform is dropped onto a defined impact surface. Most current helmet standard tests use headforms based on the EN960: 2006 [1] standard, which are made of a low resonance magnesium alloy. The standard specifies the external geometry, mass and location of the centre of gravity, but provides no inertial properties. Moreover, the biofidelity of these headforms has not been validated.

Standard headforms have changed little over the last thirty years. The first international draft standard for headforms dates back to 1970 [2], which was then superseded in 1983 [3]. Both of these documents were based on BS 1869:1960 [4], which, in turn, had been based on research first carried out by the UK's Transport and Road Research Laboratory (TRRL) in the 1950s.

As our understanding of head impact kinematics and real world accidents improves [5,6], it is becoming apparent that more sophisticated test methods and test equipment will need to be developed. Research shows that oblique impacts may be more common than radial impacts in real world accidents [7–9] with such impacts causing the head to rotate. Studies have also shown that the brain is more sensitive to rotational acceleration than translational acceleration, which can result in injuries, such as concussion, diffuse axonal injury and subdural hematoma [10,11]. If such conditions are to be evaluated in future standard tests, new headforms are likely to be required, since existing headforms have poor biofidelity in terms of their mass and inertial properties, and have not been specifically designed to model oblique impacts.

More biofidelic headforms than EN960 have been developed. The National Operating Committee on Standards for Athletic Equipment (NOCSAE) adopted a headform developed by Wayne State University [12,13] with a glycerine brain, plastic skull and rubber skin, which was intended to be more biofidelic than metal headforms [14]. It is the only standard headform with mass and inertial properties based on human cadaver data (unpublished) and is claimed

to better simulate the dynamic response of the human head. However, the NOCSAE headform has proven to be much more prone to damage than metallic ones [15] and so is unsuitable for the repeat impacts required of many automotive and sports helmet certification tests. Another headform that has been used widely for helmet research, but was originally developed as part of a vehicle frontal impact test dummy, is the Hybrid III. During its development [16], mass and moment of inertia data were obtained from embalmed cadaver studies [17–20] with an emphasis placed on measuring acceleration about the lateral axis (I_{yy}), as this data was considered to be the most important property in the design and development of a dummy to evaluate frontal impacts. This resulted in the moment of inertia of the Hybrid III head being specified along the lateral axis only (I_{yy} = 233 kg.cm^2 for the 50th percentile male) [21]. Therefore, it may not be suitable for use as a headform in oblique impact tests where the moments of inertia about each principal axis (I_{xx}, I_{yy} and I_{zz}) would need to be specified. Regardless of its physical properties, the Hybrid III head is more suitable for full dummy testing and a dedicated headform is needed for helmet certification tests. Other headforms used for automotive side impact tests include the ES-2re and the WorldSID [21], both of which specify moments of inertia (MOI) about the three principal axes. However, the MOIs for each headform differ from each other and none have been evaluated to determine their suitability for oblique helmeted impact tests.

The current authors' recent work [22] has shown that current EN960 headforms are unsuitable for oblique impact tests, as they do not have biofidelic mass and moments of inertia when compared with cadaveric data. These differences can greatly affect the oblique impact response of the headform. However, the cadaver data showed large variation. Consequently, if future certification tests should seek to evaluate helmet performance under oblique impacts, more biofidelic headforms are likely to require accurate inertia, mass distribution and centre of gravity locations that are based on an appropriate human population.

Data that currently exists has mainly come from cadaver studies. Studies published during the 1970s [19,23] show a large variation in human head physical properties. The data

show that mean human head mass is approximately 4 kg, but depending on the study, this can vary significantly. The Hybrid III, ES-2re and WorldSID dummies have head mass values of 4.5, 4 and 4.24 kg, respectively [21], all of which are consistent with the literature. EN960 standard magnesium headforms, however, have significantly greater mass. For the average size male head (size J), the mass is 4.7 kg. For a size M EN960 standard headform, which is closer in size to the Hybrid III 50th percentile male, the mass is 5.6 kg. Clearly, there is an imperative need for a more accurate and easily reproducible methodology to collect these human head physical properties.

More than a decade ago, a study by Albery and Whitestone [24] evaluated the use of computed tomography (CT) scans to determine the mass and inertial properties of the human head. The mass, centre of gravity, and MOI data were measured for 15 human cadaver heads. The heads were segmented from the neck at the occipital condyle, and the origin of each head was determined by using four anatomical landmarks as described by Becker [25]. CT scans of the heads were then collected and the heads were segmented into brain, soft tissue, and bone regions using Analyze software (Kansas, USA). By using average tissue densities published by Clauser et al. [26], the inertial properties of the segments were determined. A mean error of 2.8% and 5.2% was reported for mass and MOI, respectively, which validated the method as a means of producing a much larger human database of head physical properties. By using the same type of methodology, the initial data set produced could be constantly added to by anyone with access to head CT scans and the appropriate software. A data set such as this would be highly valuable. Decisions could be made with much more confidence as to the appropriate physical properties that should be applied to new headform designs, including for specific populations of people. To date, however, there is no published database of human head mass and inertial properties using CT imaging and segmentation software for a living population.

The present study uses a similar methodology to Albery & Whitestone [21] and builds on the current authors' previous work [22], which had shown how a new and more biofidelic

headform could be designed and built using published cadaver head mass and inertia data. In the present paper, a new database of human head physical properties is created based on a living adult population. This database could be used to inform the development of future biofidelic headforms that are specifically suitable for modelling and simulating rotational impacts about any axis.

2. Methods

The methodology of this study is based on the fact that the linear relationship between Hounsfield units derived from voxel intensity in a CT image and an object's density allows for the mass density of human tissue to be determined via radiographic imaging [21, 28]. Segmentation software is then used to automatically create a 3D volume and then a finite element model in which each element is assigned a mass density based on the corresponding Hounsfield units. Based on the Hounsfield score, the segmentation software automatically generates an optimised mesh, such that the mass distribution should accurately approximate the scanned object's density on a per voxel basis. Total mass, as well as the location of the centre of gravity and moments of inertia, are then calculated automatically by commercial software. This procedure is described in detail in the sections below.

2.1. Samples

Sixty-nine clinical head and neck Computed Tomography (CT) scans were used in the study with patients' informed consent and hospital ethics approval. All scans were screened for obvious physical abnormalities, such as tumours, head trauma and morbid obesity, with thirteen cases being excluded due to physical abnormalities. The remaining fifty-six cases included 14 females and 42 males, with a mean age of 61.7 years, a minimum age of 34 and a maximum age of 87; all were used in the study.

2.2. Segmentation

ScanIP by Simpleware (Synopsys; Dublin, Ireland) was used to import, segment, and create FE models of the scans. Each set of scans was imported as DICOM images into the software. The scans were imported in Hounsfield units, which are quantitative values for describing radiodensity in medical-grade CT scans. All CT medical images were calibrated and converted to Hounsfield units at the hospital where the scans had been obtained. The rescale intercept was 0 and the rescale slope was 1. Every set of DICOM image pixel spacing were resampled in the three XYZ planes to 0.7 mm.

Each set of scans was cropped to remove the torso, shoulders, neck, and any artefacts that were present from the CT bed. A mask was created for each head using a thresholding tool within the software. Ranges of Hounsfield values can be applied to capture which tissues or densities are needed within the mask. A range of -2000 to +3000 Hounsfield units was used for each of the masks, as this incorporates the densities of fat, craniofacial bone, skull, soft tissue, blood, water, and brain tissue [24]. It should be noted that the purpose of this procedure was only to increase computational efficiency by excluding the image background. The manual mask acts as an initial delineation of all the areas of interest, while the final model that is created subsequently remains the same, regardless of the skill of the software operator.

The head was removed from the neck at the occipital condyle. A smoothing image filter in the ScanIP software was applied on this mask to generate a more accurate and faithful surface. The filter used was a recursive Gaussian of 2.0 with binarization. Figure 1 shows a typical CT slice of one subject after segmentation, but prior to smoothing.

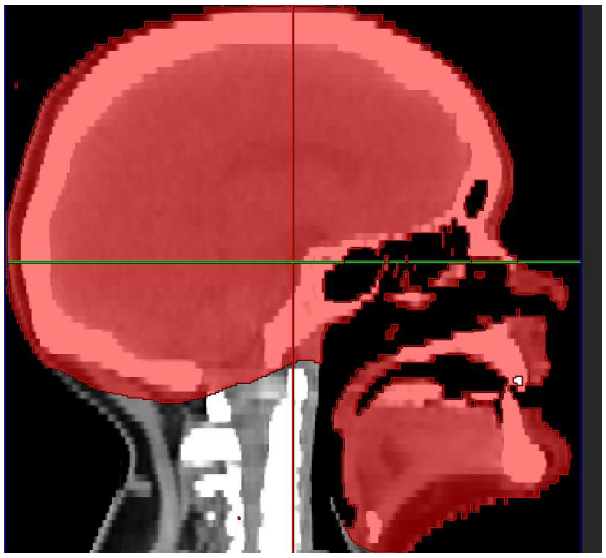

Figure 1: Mask creation and segmentation at the occipital condyle

2.3. Head Orientation and Coordinate System

Each head was then orientated to Reade's plane [21,25] and the head coordinate system was defined as shown in Fig. 2a. The origin of the coordinate system was taken to exist at the midpoint of the left and right external auditory meatus markers. The x-axis was defined to be positive anteriorly from the origin towards the midpoint between the infra-orbital notches. This aligned a subject's head in the Frankfort plane. The positive z-axis was defined by a direction from the origin toward the top of the head, perpendicular to the plane formed by the positive x-axis and the line between the auditory meatus markers. The y-axis was thus defined to be positive from the origin toward the left auditory meatus, perpendicular to the X-Z plane. The X-Z plane was considered to correspond with the mid-sagittal plane. The centre of this coordinate system was expected to be close to, but not coincident with, the physical centre of the gravity of the head.

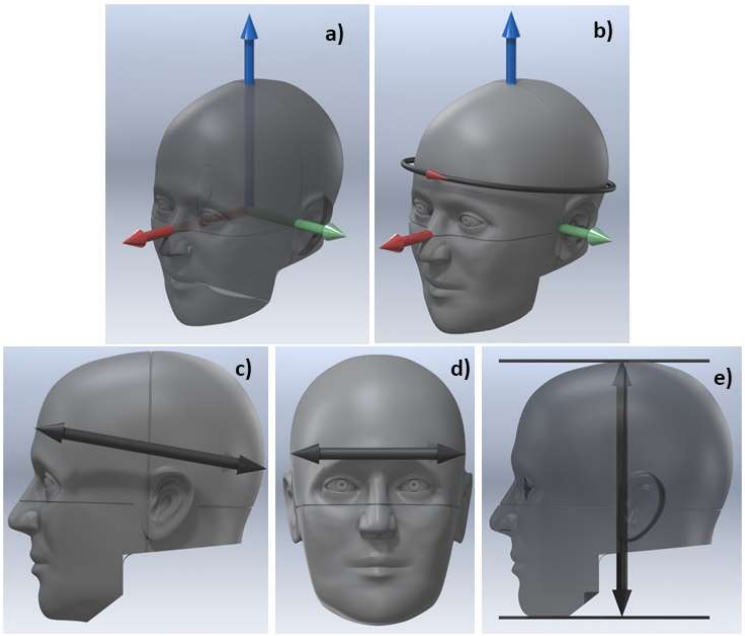

Figure 2: a). Diagram showing head orientation in the x-axis (red arrow), y-axis (green arrow) and z-axis (blue arrow) b). Head circumference measurement c). Head length measurement d). Head breadth measurement e). Head height measurement

Note that the external measurements do not correspond directly to the coordinate system.

2.4. Head Measurements

The circumference, length, breadth and height were all measured in the ScanIP software by using the paint tool. For circumference, this was used to draw a central axis through the centre of the head. A cross-sectional measurement was then taken around the head. The circumference measurement was taken from just above the eyebrows and around to a point on the head just above the ears [27], as illustrated in Fig. 2b. Head length was measured using the paint tool to draw a line from the back of the head to a point above the eyebrows in the sagittal plane. This line was drawn along the same direction as the circumference of the head, as noted in Fig. 2c. Head breadth was measured by drawing a line from just above the ears on the left side of the head to just above the ears on the right side of the head in the transverse plane, as noted in Fig. 2d. Head height was measured by drawing tangential lines to the top

of the head and the bottom of the chin, and a perpendicular line joining the two. The head height was then measured by this perpendicular line, as illustrated in Fig. 2e.

2.5. Finite Element (FE) Model

An individual finite element (FE) model was created in ScanIP for each of the 56 heads and the segmented 'Head' object was dragged into the model. Greyscale values were used for smart mask smoothing in the pre-processing step. The coordinate system was exported globally.

To calculate the mass density values, a mapping function was determined using known Hounsfield unit (HU) values and the corresponding mass density values reported in the literature (See Table 1 for HU and mass density values used) [28]. Figures 3 and 4 show the corresponding mapping functions for negative and positive Hounsfield unit values, respectively, which relate to tissue for which the relative density (specific gravity) is either less than or greater than unity.

Table 1: Hounsfield unit (HU) and corresponding mass density used to derive FE model mapping functions [28]

HU	Mass Density (g/cm^3)
-1000	0.01
-773	0.19
-516	0.49
-72	0.95
-34	0.98
-4	1
42	1.04
49	1.05
238	1.12
951	1.5
2000	2

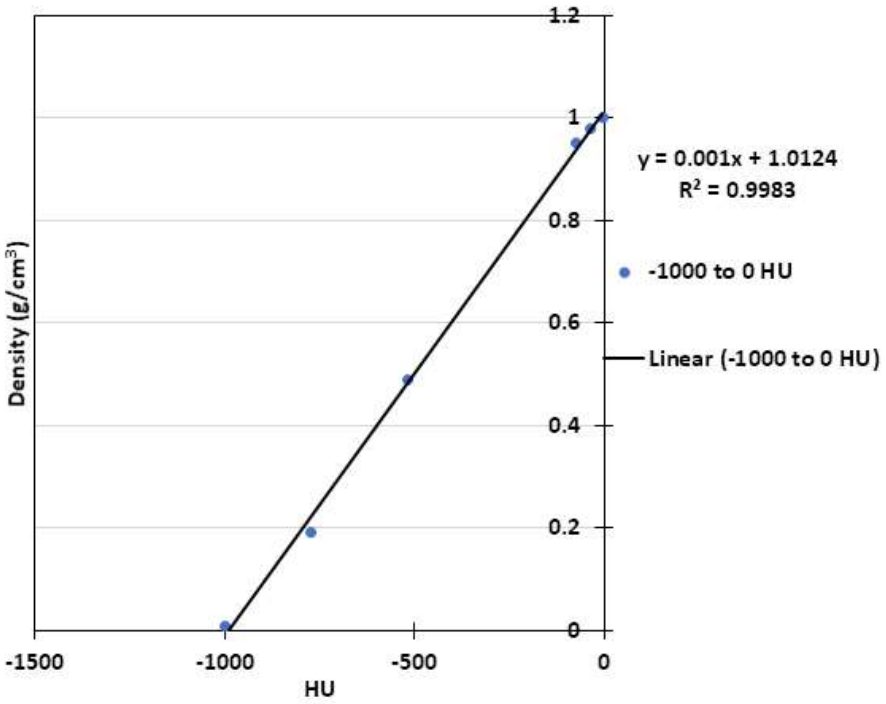

Figure 3: Mass density vs. Hounsfield Units (HU) between -1000 and 0 HU.

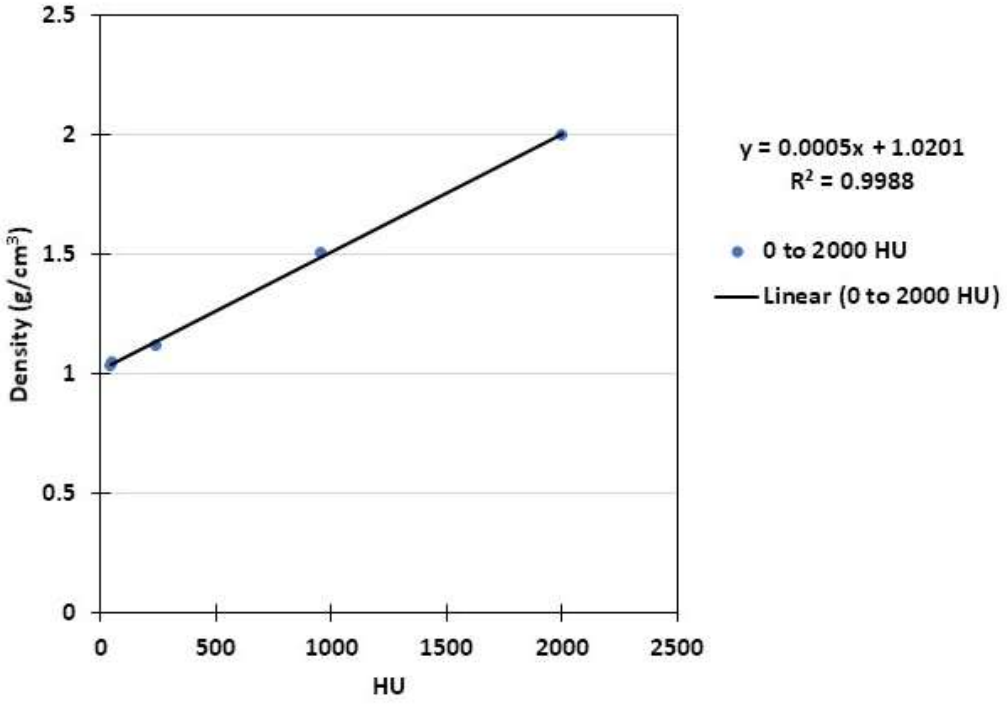

Figure 4: Mass density vs. Hounsfield Units (HU) between 0 and 2000 HU.

The software calculates mass density per pixel using the following formula shown in Eq. (1):

$$Mass\ Density = m * GS + c \qquad (1)$$

where m and c are corresponding coefficients taken from the mapping functions shown in Figs. 3 and 4 (i.e., slope of the line and y-axis intercept, respectively), and 'GS' are the greyscale values, which in this case are the Hounsfield unit values. When the FE model was configured to the above settings and generated, mass and inertial properties were calculated automatically by the ScanIP software (see Fig. 5).

This method was validated directly using two fresh porcine heads. Masses predicted by this modelling approach that used the corresponding CT scans and associated FE models differed from the experimentally measured masses by less than 1%. Each element in the FE models had only two parameters that could influence the overall model mass and inertial properties, namely its assigned mass density value and its volume. Since both are known accurately, the calculated mass distribution of the head was also an accurate representation of the physical head.

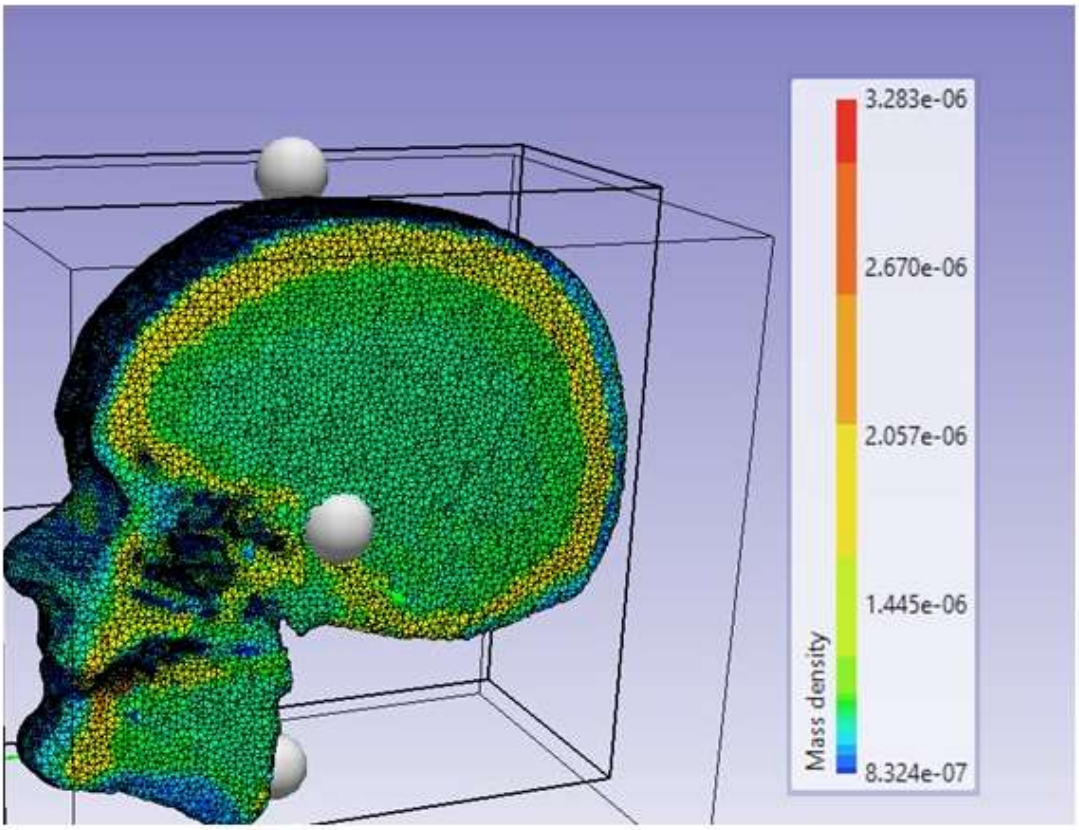

Figure 5: Finite element model section showing mass distribution of the model

3. Results

3.1. CT Head Data Set

FE models were successfully created for 56 living subjects and physical properties calculated and recorded for each. Table 2 shows the mean, minimum, maximum and standard deviation for each parameter recorded. Appendix A presents this specific data for all 56 subjects.

Table 2: Mean, minimum, maximum and standard deviations for CT head mass, circumference, CG, MOI, length, breadth and height. Refer to Fig. 2 for definition of axes. N = 56

	Age	Mass (kg)	Circ. (cm)	CG_x (mm)	CG_y (mm)	CG_z (mm)	I_{xx} (kg cm^2)	I_{yy} (kg cm^2)	I_{zz} (kg cm^2)	Length (cm)	Breadth (cm)	Height (cm)
Mean	61.71	4.02	57.38	11.86	1.43	28.03	188.62	200.36	130.21	19.86	15.99	21.42
Min	34.00	3.10	52.29	0.46	8.78	14.80	119.94	127.40	84.90	17.97	14.38	17.92
Max	87.00	4.88	61.79	25.16	7.24	39.69	251.14	271.46	184.44	21.90	19.53	25.40
SD	12.01	0.45	2.18	5.75	3.43	5.71	36.34	37.09	24.57	0.82	0.86	1.56

3.2. Head Mass Measured Via CT and FE Models

Head masses calculated from these 56 CT based FE models show a reasonably close match to the previously published cadaver data [17,29,30]. Both sets of data are presented in Fig. 6 along with corresponding least squares fit lines. The linear relationships between head mass and circumference from the CT method and previously published cadaver data yield R^2 values of 0.74 and 0.77, respectively.

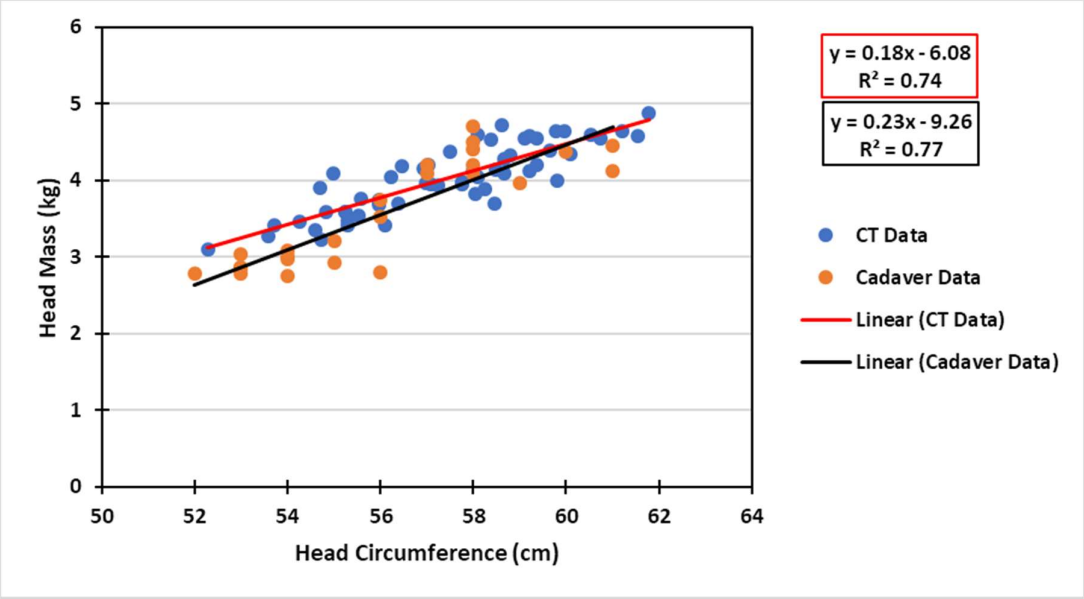

Figure 6: Head mass vs. head circumference for both published cadaver data [17, 29, 30] and the present CT data

Table 3: Mass values for standard headform circumference sizes as calculated using the equations from Fig. 6 for published cadaver data [17, 19, 30] and the present CT data. Percentage difference in brackets.

Headform Size	Head Circumference (cm)	Cadaver Head Mass (kg)	CT Head Mass (kg)	Percentage Difference (%)
A	49.5	2.1	2.8	28.6
C	51.5	2.5	3.1	21.4
E	53.5	3.0	3.5	15.4
J	57.5	3.9	4.2	7.4
M	60.5	4.6	4.7	2.2
O	62.5	5.1	5.1	0
HIII	59.0	4.3	4.5	4.5

3.3. Moment of Inertia (MOI) Measured via CT and FE Models

Again, head MOI values calculated from the present CT based FE models and presented in Figs. 7-9 closely match the published cadaver data [23, 31, 32]. Using the least squares equations from Figs. 7 - 9, values for the I_{xx}, I_{yy}, and I_{zz} MOIs were calculated for standard size headforms and the Hybrid III 50th percentile male and are summarised in Tables 4-6.

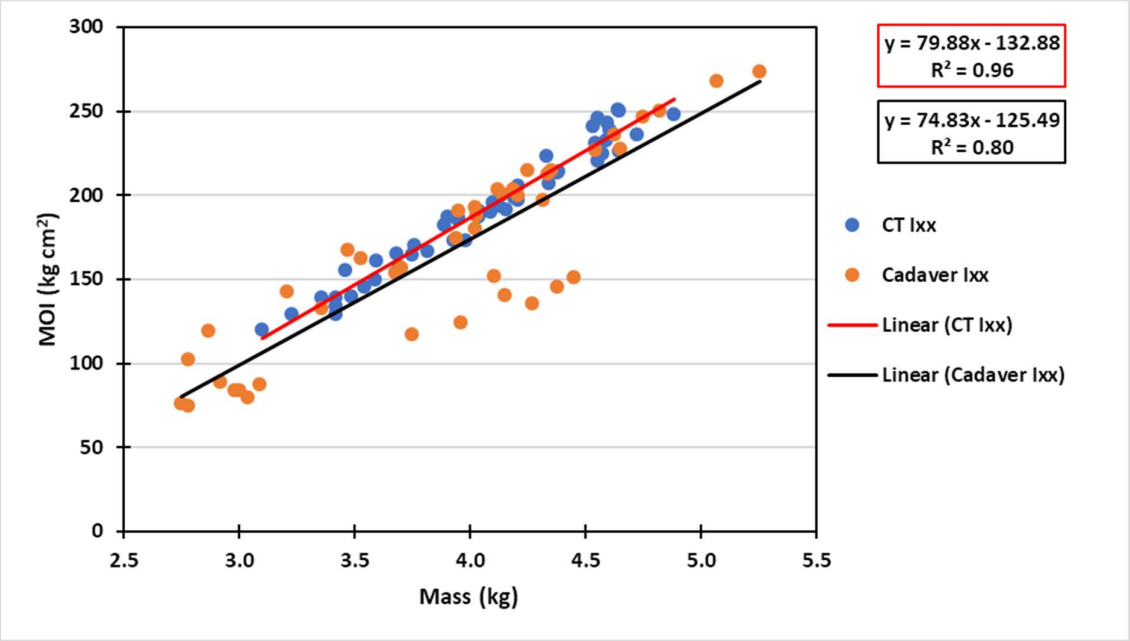

Figure 7: Head MOI (I_{xx}) vs. head mass based on the present CT data and published cadaver data *[23,31,32]*

Table 4: Calculated standard headform MOI (I_{xx}) values using the least squares fit equations from Fig. 7 for the headform sizes in Table 3 according to published cadaver data and the present CT data. Percentage difference shown in brackets.

Headform Size	I_{xx} via Cadaver Eq. ($kg.cm^2$)	I_{xx} via CT Eq. ($kg.cm^2$)	Percentage Difference (%)
A	31.7	90.8	96.6
C	61.6	114.7	60.3
E	99.0	146.7	38.8
J	166.3	202.6	19.7
M	218.7	242.6	10.3
O	256.1	274.5	6.9
HIII	196.3	226.6	14.3

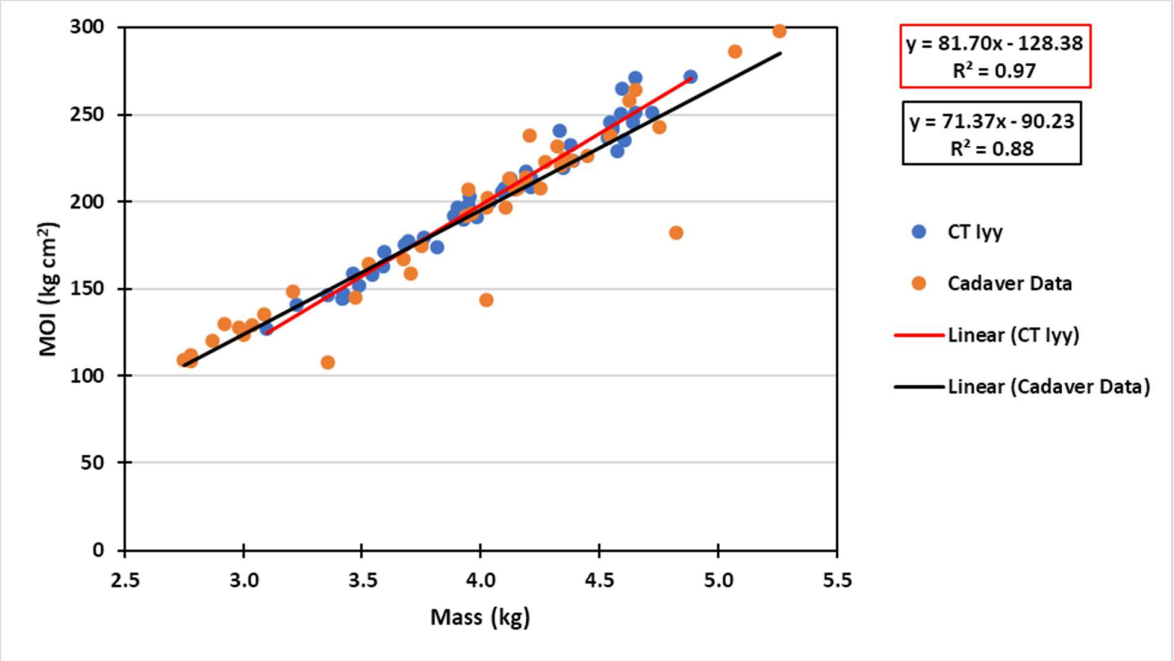

Figure 8: Head MOI (I_{yy}) vs. head mass based on the present CT data and published cadaver data *[23,31,32]*

Table 5: MOI (I_{yy}) values for standard size headforms as calculated using the least squares equations from Fig. 8 based on published cadaver data and the present CT data. Percentage difference shown in brackets.

Headform Size	I_{yy} via Cadaver Eq. ($kg.cm^2$)	I_{yy} via CT Eq. ($kg.cm^2$)	Percentage Difference (%)
A	59.6	100.4	50.9
C	88.2	124.9	34.4
E	123.9	157.6	23.9
J	188.1	214.8	13.2
M	238.1	255.6	7.1
O	273.8	288.3	5.2
HIII	216.7	239.3	9.9

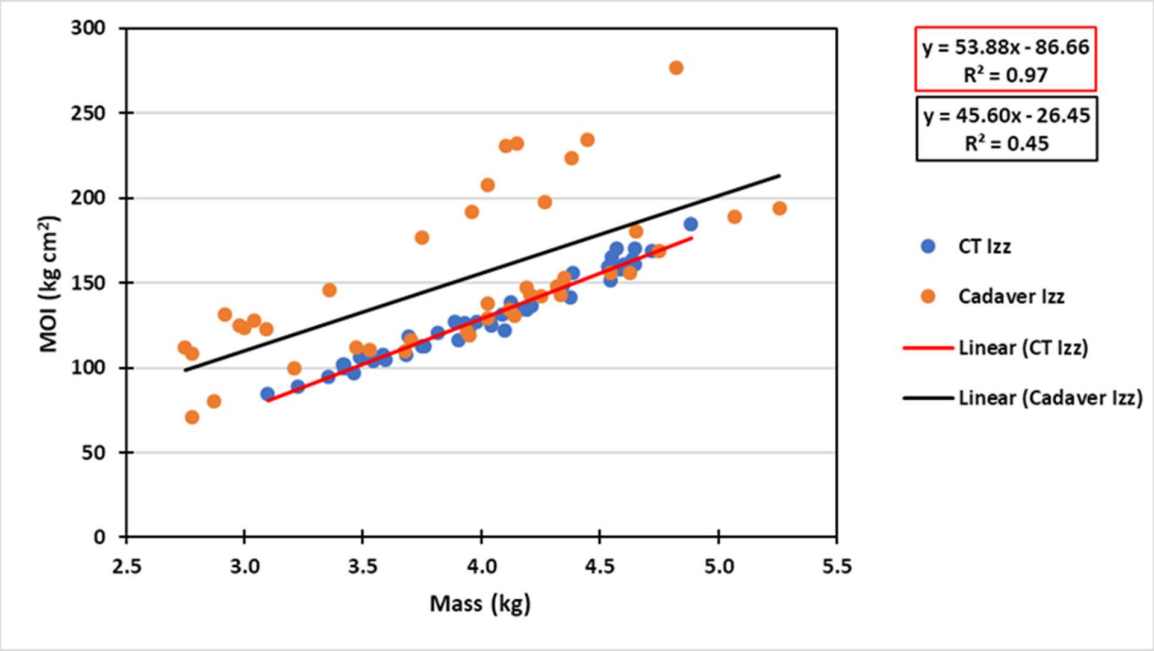

Figure 9: Head MOI (I_{zz}) vs. head mass based on the present CT data and published cadaver data *[23,31,32]*

Table 6: MOI (I_{zz}) values for standard size headforms as calculated using the least squares fit equations from Fig. 9 based on published cadaver data and the present CT data. Percentage difference shown in brackets.

Headform Size	I_{zz} via Cadaver Eq. ($kg.cm^2$)	I_{zz} via CT Eq. ($kg.cm^2$)	Percentage Difference (%)
A	69.3	64.2	7.6
C	87.6	80.4	8.6
E	110.4	101.9	7.9

J	151.4	139.6	8.1
M	183.3	166.6	9.6
O	206.1	188.1	9.1
HIII	169.6	155.8	8.5

3.4. Centre of Gravity (CG) Location Measured Via CT and FE Models

The CG is not coincident with the origin of the XYZ coordinate reference system indicated in Fig. 2. In reality, the CG is a few cms from this datum in the X and Z directions, and within a cm from the origin in the Y direction. In general, CG locations calculated from the 56 CT scanned heads correspond well with the locations reported in the literature (see Fig. 10). Mean values differ most in the X direction (by 6.01 mm). However, mean values in the Y and Z direction only differ by 0.8 mm and 1.56 mm, respectively (see Table 7).

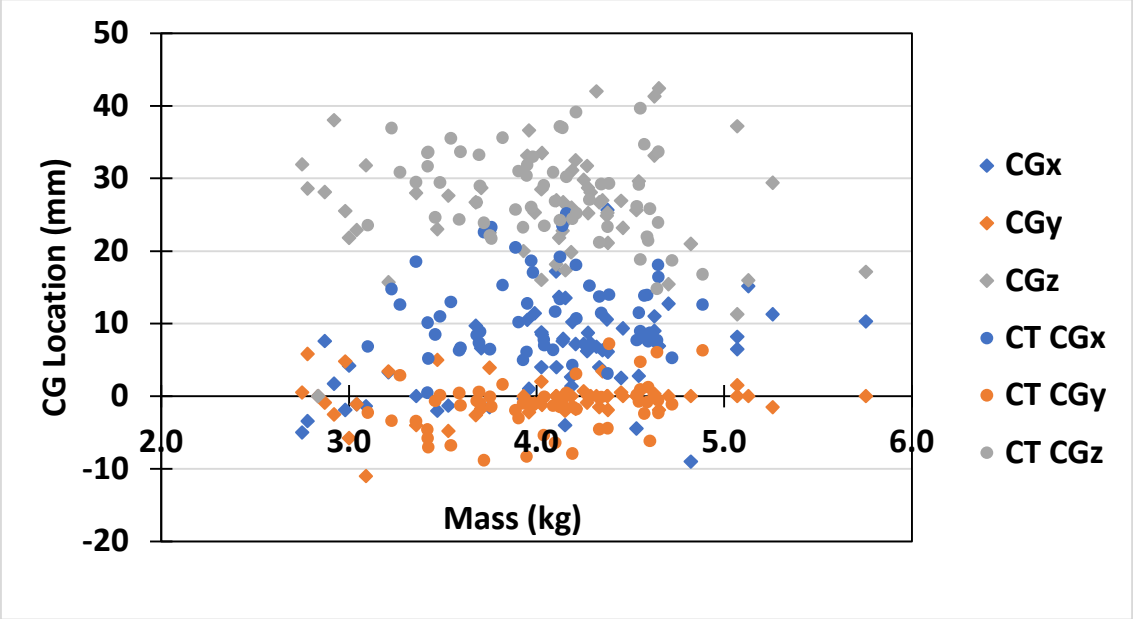

Figure 10: CG location for published cadaver studies [23, 31, 32] (diamond dots) and the present CT head data (circular dots). Note these distances are relative to the origin, as defined by the x- y- and z-axes in Fig. 3 and Section 2.3.

Table 7: Location of CG as identified by the present 56 CT scans of living subjects and published cadaver data, along with corresponding standard deviation and extrema. Note these distances are relative to the origin, as defined by the XYZ axes in Fig. 2 and Section 2.3.

	CG_x, CT data (mm)	**CG_y**, CT data (mm)	**CG_z**, CT data (mm)	**CG_x**, Cadaver data (mm)	**CG_y**, Cadaver data (mm)	**CG_z**, Cadaver data (mm)
Mean	11.69	-1.33	28.13	5.68	-0.53	26.57
Std. Dev.	5.58	3.47	5.71	6.16	2.50	7.54
Minimum	0.46	-8.78	14.80	-9.00	-11.00	11.00
Maximum	25.16	7.24	39.69	25.68	5.80	42.40

4. Discussion

For obvious reasons, helmet certification tests cannot use real human heads. Thus, surrogates will always be required to simulate head impact. Headforms that are used today currently represent the state of the art method to test helmets, as their design and construction are robust, cost effective and provide good repeatability in terms of impact response in laboratory conditions. However, the data from the present study show that these headforms could be more biofidelic in terms of the absolute mass, mass distribution, and moments of inertia. In general, the relationships that have been established in the present work between head circumference and mass, as well head MOI and mass, show sufficiently good linearity. As a result, simple linear models can be used to estimate the mass and inertia properties of differently sized heads from a single measurement of head circumference. Calculated masses for standard head sizes show significant differences when compared to actual current headform masses, which highlights the limited biofidelity of current headforms. This is unsurprising given that the geometry-mass relationships were determined from human data, while the headforms are made of non-biological materials, which may not be representative of actual head masses. This further highlights the limited biofidelity of current headforms, indicating that there may be a need to improve the biofidelity of current headforms in terms of their mass and inertial properties. The existing EN960 headform designs can be adapted relatively easily to improve their mass and inertial biofidelity.

Indeed, the authors' recent work involved designing a new PPLA-M headform [22], which demonstrates how the present CT data can be used to create more biofidelic headforms. That headform [22] was originally designed to evaluate helmets in oblique impacts and has proven to be robust even after having been used for thousands of impacts. Although it is a 3D printed headform, its impact response has remained unchanged over its lifetime thus far. The total material cost was less than £100 and, although a new standard headform is unlikely to be manufactured via a 3D printing process, when compared with current magnesium headforms which cost in excess of £1000, it represents good economic value. A headform that could be manufactured more cheaply would possibly be adopted more widely and accepted as a replacement for current, less biofidelic headforms. Changes in standard headforms are likely to be incremental and improving mass and MOI is the logical next step. In this regard, the authors' recent work using the PPLA-M represents a significant improvement in headform biofidelity.

As stated previously, the data on which the PPLA-M design was based shows large variation and comes from multiple studies [17, 18, 21, 23, 29, 32]. Not all parameters were recorded for each head. Thus, the data set is unreliable and cannot be considered as representative of the population. The present method developed in Section 2 demonstrates how the presented database of human head physical properties could be improved (e.g., increase database of cases in Appendix A), while the results presented in Section 3 display notably less variation than previously published cadaver data. Furthermore, the determination of simple empirical geometry-mass-MOI relationships means that future studies can employ these relationships to determine mass/inertial properties on a patient-specific basis, using only external geometric head measurements.

CT based FE model data presented in Appendix A represents the first human head physical property data heretofore published that is based on a living population. Comparing CT and cadaver mass data shows good agreement, although there are some significant

differences. For example, CT mass data for a size A head shows a 28.6% difference than a cadaver head of the same size (see Table 3). Using the two equations of linear fit from Fig. 6, head masses were estimated for standard size headforms and the Hybrid III 50th percentile male headford. The largest difference between the data sets is for the smallest head sizes where, for a size A head, the CT mass of 2.8 kg (i.e., that estimated from the linear fit to the present 56 CT scanned subjects) is 0.7 kg heavier than the linear fit predicted by published cadaver data for a head of the same size (i.e., 2.1 kg). This difference reduces as head size increases and there is no difference in mass at all for size O heads (see Table 3). Note that the actual mass of the HIII headform is 4.5 kg, which matches that predicted by the equation from the present CT head data.

Comparing CT and cadaver MOI shows a similar trend for moment of inertia about the x and y-axes with the largest differences for size A heads of 96.6% and 50.9% for the x and y-axes, respectively. This difference drops to 6.9% and 5.2% for the x and y-axes, respectively, for size O heads. The opposite is true of the z-axis data, for which the largest difference is for the larger head sizes (9.6% for size M and 9.1% for size O). The head MOI-mass linear relationship based on CT data and cadaver data yield R^2 values: 0.96 and 0.80, respectively, (see Fig. 7) for I_{xx}; 0.97 and 0.88, respectively, (see Fig. 8) for I_{yy}; and 0.97 and 0.45, respectively, (see Fig. 9) for I_{zz}. In all cases, the present CT data shows a significantly stronger data fit than the meta analysis of the previously published cadaver data. This is unsurprising since the same methodology has been used on the present dataset of 56 living subjects, whilst the cadaver data is a synthesis of data from various published sources that did not use consistent methodology. Notably, the z-axis estimates of MOI are worst when based on the previously published cadaver data [22].

Comparing CT and cadaver CG locations also showed good agreement in general. Comparing the means shows the greatest difference in the x direction (6.01 mm). Differences in the y and z directions were 0.8 mm and 1.56 mm, respectively. It is important to have the

most accurate data possible, since mass, inertia and CG location parameters can greatly influence the oblique impact response of headforms [22].

The advantage of using the present CT data collection method is that each sample is always from a living subject. Cadaver heads can lose fluid after segmentation, while some heads are embalmed or frozen, which can also alter the results. This is not an issue with the CT method. For the first time ever, this paper has presented a database (Appendix A) that contains the physical properties of 56 different adult heads. This database can either be used in its present form or as the basis for subsequent expansion. As it stands, it is somewhat limited in that most subjects are older males, and all are western European Caucasians (Irish). In the future, additional cases using the present methodology might usefully include more females, a greater range of ages and more ethnic groups. This would allow for a more segmented analysis and would show the extent to which gender, age or ethnic specific headforms might be required. Regardless, a much larger data set will guarantee that more biofidelic headforms could be designed and built.

While it is possible to create simple linear models based on published cadaver data and thus to build a more biofidelic headform in terms of its mass and inertia, it is significantly more accurate to do so using CT data from a population of living subjects. Cadaver data show large variation and physical property parameters can have a large influence on the oblique response of a headform. The CT data collection method described in this paper represents a means by which the current published data set can be expanded. The key equations from the present CT dataset relate a person's head mass, CG location and three moments of inertia simply in terms of their head circumference.

5. Conclusions

It is possible to significantly improve the biofidelity of current standard headforms in terms of their mass and moments of inertia without compromising the headform durability or cost. The

method described in this paper to collect physical properties of the human head is an accurate means by which the current published data set could be increased. The data set presented in this paper now provides a basis for the design of more biofidelic future headforms. The linear equations associated with this new primary dataset relate head circumference to head mass (Fig. 6) and moments of inertia (Figs. 7-9):

Head Mass = 0.18 * Head Circumference – 6.08

I_{xx} = 79.88 * Head Mass – 132.88

I_{yy} = 81.70 * Head Mass – 128.38

I_{zz} = 53.88 * Head Mass – 86.66

where mass is in kg and circumference is in cm and I is in kg.cm^2. Mean average head centre of gravity locations are not coincident with the origin of the XYZ axes; instead they are some few cms away from this location (Table 7):

CG_x = 11.69 mm; CG_y = -1.33 mm; CG_z = 28.13 mm

Acknowledgements

The authors would like to acknowledge Margaret Moore, University Hospital Galway for organizing access and training on the CT systems. Funding was provided by the European Union's Horizon 2020 research programme under Marie Sklodowska – Curie grant agreement No. 642662. Figure 2 was created using files under licence from NOCSAE.

References

[1] EN 960: 2006. Headforms for use in the testing of protective helmets. British Standards Institution; 2006.

[2] ISO/R 1511:1970. Protective helmets for road users. International Organisation for Standardisation; 1970.

[3] ISO/DIS 6220:1983. Headforms for use in the testing of protective helmets. International Organisation for Standardisation; 1983.

[4] BS 1869:1960. Specification for protective helmets for racing motorcyclists. British Standards Institution; 1960.

[5] Gilchrist MD, editor. IUTAM Symposium on Impact Biomechanics: From fundamental insights to applications. Dordrecht: Springer; 2005.

[6] Rueda MAF, Halley WL, Gilchrist MD. Fall and injury incidence rates of jockeys while racing in Ireland, France and Britain. Injury. 2010;41:533–539.

[7] Bourdet N, Deck C, Serre T, et al. In-depth real-world bicycle accident reconstructions. International Journal of Crashworthiness. 2014;19:222–232.

[8] Rueda F, Cui L, Gilchrist MD. Finite element modelling of equestrian helmet impacts exposes the need to address rotational kinematics in future helmet designs. Computer Methods in Biomechanics and Biomedical Engineering. 2011;14:1021–1031.

[9] Gilchrist MD. Modelling and accident reconstruction of head impact injuries. Key Engineering Materials. Trans Tech Publ; 2003. p. 417–432.

[10] Deck C, Willinger R. Improved head injury criteria based on head FE model. International Journal of Crashworthiness. 2008;13:667–678.

[11] Kleiven S. Predictors for traumatic brain injuries evaluated through accident reconstructions. Stapp Car Crash Journal. 2007;51:81–114.

[12] Cobb BR, MacAlister A, Young TJ, et al. Quantitative comparison of Hybrid III and National Operating Committee on Standards for Athletic Equipment headform shape characteristics and implications on football helmet fit. Proceedings of the Institution of Mechanical Engineers, Part P: Journal of Sports Engineering and Technology. 2015;229:39–46.

[13] Hodgson VR. National Operating Committee on Standards for Athletic Equipment football helmet certification program. Medicine and Science in Sports. 1975;7:225–232.

[14] National Operating Committee on Standards for Athletic Equipment. Standard test method and equipment used in evaluating the performance characteristics of headgear/equipment. National Operating Committee on Standards for Athletic Equipment; 2017.

[15] Newman J. The biomechanics of head trauma and the development of the modern helmet. How far have we really come? Proceedings of the IRCOBI Conference. 2005.

[16] Backaitis SH, Mertz HJ. Hybrid III: The First Human-like Crash Test Dummy. Society of Automotive Engineers; 1993.

[17] Mertz HJ, Patrick LM. Investigation of the kinematics and kinetics of whiplash [Internet]. Warrendale, PA: SAE International; 1967. p. 1–29. Report No.: 670919. Available from: https://doi.org/10.4271/670919.

[18] Hodgson VR, Thomas LM. Breaking strength of the human skull vs. impact surface curvature. Detroit: U.S. Department of Transportation, National Highway Traffic Safety Administration; 1973.

[19] Reynolds HM, Clauser CE, McConville J, et al. Mass Distribution Properties of the Male Cadaver [Internet]. Warrendale, PA: SAE International; 1975. Report No.: 750424. Available from: http://papers.sae.org/750424/.

[20] B. Walker Jr L, H. Harris E, R. Pontius U. Mass, Volume, Center of Mass and Mass Moment of Inertia of Head and Head and Neck of the Human Body. 1973.

[21] Yoganandan N, Pintar FA, Zhang J, et al. Physical properties of the human head: Mass, center of gravity and moment of inertia. Journal of Biomechanics. 2009;42:1177–1192.

[22] Connor TA, Stewart M, Burek R, et al. Influence of headform mass and inertia on the response to oblique impacts. International Journal of Crashworthiness. 2018;1–18.

[23] Chandler RF, Clauser CE, McConville JT, et al. Investigation of Inertial Properties of the Human Body [Internet]. Air Force Aerospace Medical Research Lab Wright-Patterson AFB OH; 1975. p. 1–171. Report No.: AMRL-TR-74-137. Available from: http://www.dtic.mil/docs/citations/ADA016485.

[24] Albery CB, Whitestone JJ. Comparison of Cadaveric Human Head Mass Properties: Mechanical Measurement vs. Calculation from Medical Imaging. Proc. of the 31st International Workshop Injury Biomechanics Research, 157. 2003.

[25] Becker EB. Measurement of mass distribution parameters of anatomical segments. SAE Transactions. 1972;2818–2833.

[26] Clauser CE, McConville JT, Young JW. Weight, volume, and center of mass of segments of the human body. Antioch Coll Yellow Springs OH; 1969.

[27] Harris SR. Measuring head circumference: Update on infant microcephaly. Canadian Family Physician. 2015;61:680–684.

[28] Kang J, Lee DJ. Development of DICOM Convert Program for the Geant4 Monte Carlo Simulation of the Radiotherapy. Progress in Medical Physics. 2013;24:259–264.

[29] Ching RP. Relationship between head mass and circumference in human adults. Seattle, WA, USA: University of Washington; 2007.

[30] Hodgson VR, Thomas LM. Breaking strength of the human skull vs. impact surface curvature. 1972.

[31] Plaga JA, Albery C, Boehmer M, et al. Design and Development of Anthropometrically Correct Head Forms for Joint Strike Fighter Ejection Seat Testing. Air Force Research Lab Wright-Patterson AFB OH Human Effectiveness Directorate; 2005.

[32] Beier G, Schuller E, Schuck M, et al. Center of gravity and moments of inertia of human heads. HS-030 722, “International IRCOBI Conference on the Biomechanics of Impacts (5th) Proceedings” [Internet]. Amsterdam; 1980 [cited 2018 Jan 25]. p. 218–228. Available from: https://trid.trb.org/view/185516.

Appendix A

Table A1: CT living subject human head physical property database.

Subject name	Sex	Age	Head Mass_kg	Head Circ. (cm)	CG_x (mm)	CG_y (mm)	CG_z (mm)	I_{xx} [kg.cm^2]	I_{yy} [kg.cm^2]	I_{zz} [kg.cm^2]	Head Length (cm)	Head Breadth (cm)	Head height (cm)
P1	M	66	3.49	55.31	10.98	0.12	29.44	140.28	151.86	106.08	19.79	15.64	21.26
P2	M	42	3.93	57.23	5.01	-0.99	23.26	173.04	189.51	126.39	19.92	15.22	22.47
P3	M	74	4.19	56.45	4.30	-7.88	24.46	198.69	217.26	134.02	19.78	15.73	21.65
P4	M	59	4.60	58.11	8.74	-6.14	25.82	239.09	234.91	160.74	19.46	16.94	25.40
P5	M	74	4.72	58.63	5.27	-1.10	18.71	236.48	250.95	168.70	20.00	16.60	22.39
P6	M	55	4.21	59.37	10.70	-1.76	25.22	197.44	208.17	141.99	20.70	17.39	22.15
P7	M	69	4.04	56.24	7.03	-0.05	23.45	187.09	200.43	125.12	19.09	15.36	21.42
P8	F	64	3.42	53.72	5.18	-7.04	33.61	129.28	145.01	99.65	19.05	14.73	20.18
P9	M	65	3.59	55.24	6.32	0.43	24.35	149.95	162.65	107.63	18.80	15.43	22.50
P10	M	46	4.38	57.50	3.13	-4.43	23.35	213.53	232.72	141.77	20.22	15.99	21.91
P11	M	58	3.75	55.96	6.47	-0.05	22.14	164.53	175.22	112.88	19.52	15.30	20.72
P12	M	87	4.88	61.79	12.61	6.31	16.78	248.57	271.46	184.44	21.90	16.27	22.40
P16	M	41	4.59	60.54	7.57	1.25	21.44	243.23	265.04	159.35	21.43	15.64	22.89
P17	M	79	4.64	59.77	7.71	6.06	14.80	251.14	245.80	163.46	20.01	16.78	22.54
P18	M	36	3.95	57.77	6.10	-8.30	30.38	186.14	198.06	123.57	20.01	15.43	21.77
P19	M	60	4.59	59.21	13.96	-0.81	22.00	232.57	250.56	157.68	20.42	15.64	23.59
P20	M	79	4.55	59.10	8.05	4.75	18.81	245.92	241.47	160.04	20.06	16.16	22.75
P21	F	60	3.42	56.10	0.46	-4.58	33.54	134.65	144.69	102.17	19.18	15.57	19.11
P22	F	58	3.46	54.26	8.53	-0.66	24.62	155.71	158.97	96.94	18.55	15.72	18.41
P23	F	45	4.09	58.67	6.39	-1.30	30.83	190.44	205.65	131.65	20.54	15.92	21.35
P24	F	56	3.10	52.29	6.84	-2.27	23.56	119.94	127.40	84.90	17.97	14.49	17.92
P25	F	58	3.59	54.83	6.66	-1.28	33.64	161.03	171.55	104.85	19.32	14.94	20.44
P26	M	71	4.57	61.54	13.85	-2.39	34.68	224.84	229.04	169.95	20.97	17.39	21.63
P27	M	65	4.10	55.00	11.67	-6.40	26.86	196.21	207.65	122.28	18.64	15.31	19.39
P28	F	68	3.82	58.05	15.30	1.65	35.61	167.21	173.89	120.31	20.13	16.29	19.25
P29	F	77	3.68	55.98	8.44	-0.64	26.71	165.43	175.48	107.43	19.53	19.53	20.16

P30	M	34	4.04	58.09	7.83	-5.36	29.05	190.68	199.93	128.09	20.18	16.27	21.42
P31	M	79	4.53	58.39	7.74	0.17	26.18	241.44	236.89	159.14	19.92	15.36	22.68
P32	M	76	3.69	58.46	7.37	0.62	33.26	157.60	177.39	118.50	20.71	15.50	22.77
P33	F	74	3.23	54.72	14.75	-3.38	36.95	129.49	140.77	89.11	19.14	14.52	20.40
P34	M	53	4.12	59.22	13.40	-0.25	37.15	194.06	212.98	138.62	20.64	16.06	23.03
P35	M	58	4.55	60.74	8.99	0.93	39.69	221.04	243.74	165.30	21.21	17.05	24.22
P36	F	49	3.42	55.30	10.11	-5.80	31.69	139.26	147.36	101.93	19.21	15.55	20.44
P37	M	46	3.95	57.09	12.80	-0.94	31.88	186.95	202.87	123.53	19.98	16.34	23.92
P38	F	59	3.54	55.53	13.01	-6.79	35.51	146.01	158.36	103.95	19.50	15.15	20.30
P39	M	53	4.54	59.38	11.50	-0.74	29.13	231.35	245.80	151.54	20.73	16.48	20.09
P40	M	65	3.90	54.71	10.20	-2.99	31.00	187.17	196.77	116.05	18.66	15.78	22.12
P41	M	76	4.39	59.66	13.98	7.24	29.29	214.12	223.85	156.15	19.85	17.14	22.08
P42	M	58	4.65	61.20	16.42	-2.30	33.66	226.37	250.77	170.01	21.11	17.14	24.22
P43	M	53	4.33	58.79	13.74	-4.53	21.20	223.66	240.93	147.03	20.60	15.85	20.58
P44	M	62	4.65	59.95	18.10	-0.58	23.94	250.65	271.17	161.13	20.97	16.20	22.89
P45	M	56	4.14	58.48	23.48	-0.85	36.96	200.23	208.91	134.98	20.18	16.55	22.47
P46	M	75	4.16	56.92	25.16	0.44	30.23	191.41	208.47	134.29	20.24	15.92	21.42
P48	M	66	4.34	60.09	11.45	-0.10	29.21	207.39	219.64	149.02	20.74	16.97	20.02
P49	M	38	4.21	57.04	18.09	3.07	39.14	206.12	213.70	136.73	19.21	16.62	22.40
P50	F	61	3.36	54.60	18.56	-3.43	29.48	139.65	146.66	94.65	18.70	15.29	20.37
P51	F	45	3.98	57.75	17.05	-1.23	32.99	173.04	191.10	127.24	20.56	15.50	19.46
P52	M	67	3.76	55.57	23.25	-1.41	21.73	170.41	179.21	112.85	18.99	15.82	19.67
P54	M	68	3.89	58.25	20.50	-1.93	25.70	182.42	191.64	126.71	20.09	16.48	20.58
P55	M	67	4.12	58.00	19.21	-1.48	24.26	184.65	200.74	135.83	20.35	15.69	20.72
P56	M	70	3.97	56.97	18.68	-0.96	26.04	190.19	201.24	125.87	19.48	16.06	23.10
P57	M	63	3.70	56.37	8.87	-0.99	28.97	162.01	170.59	112.27	19.40	15.78	21.24
P58	M	66	4.28	58.66	15.23	-0.11	27.07	206.21	217.83	146.82	19.94	16.83	21.91
P59	M	67	3.72	55.96	22.58	-8.78	23.87	171.47	177.47	111.39	18.89	15.51	19.11
P60	F	64	3.27	53.58	12.60	2.87	30.86	129.98	145.01	91.31	19.18	14.38	20.02
P62	M	76	3.58	55.26	22.24	-2.99	25.23	155.38	162.96	107.75	18.85	15.98	20.02